

Supporting Online Material for

Trifurcate Feed-Forward Regulation of Age-Dependent Cell Death Involving *miR164* in *Arabidopsis*

Jin Hee Kim, Hye Ryun Woo, Jeongsik Kim, Pyung Ok Lim, In Chul Lee, Seung Hee Choi, Daehee Hwang, Hong Gil Nam*

*To whom correspondence should be addressed. E-mail: nam@postech.ac.kr

Published 20 February 2009; *Science* **323**, 1053 (2009)
DOI: 10.1126/science.1166386

This PDF file includes:

Materials and Methods
Figs. S1 to S9
Tables S1 and S2
References

Supporting Online Material

Materials and Methods

Plant materials and growth conditions

Arabidopsis thaliana plants were grown in an environmentally controlled growth room (Korea Instruments, Seoul, Korea) at 22 °C with a 16 h light/8 h dark cycle. All experiments were carried out using third and fourth rosette leaves. Leaf samples were obtained by cutting leaves at approximately the middle of the petiole with a sharp scalpel to minimize wounding effects.

Measurement of photochemical efficiency and membrane ion leakage

The photochemical efficiency of photosystem II (PS II) and membrane ion leakage values were measured with a Plant Efficiency Analyzer (Hansatech Instruments, Morfolk, UK) and a 712 ConductoMeter (Metrohm, Herisau, Switzerland), respectively, as described previously with minor modifications (S1).

Histochemistry

To visualize dying cells, leaves were detached and submerged in 0.05% lactophenol-trypan blue solution (0.05% trypan blue, 25% (w/v) lactic acid, 25% water-saturated phenol, and 50% ethanol). The samples were washed in chloral hydrate solution (2.5 g/µL) to reduce background staining, and photographed using a SZX9 stereomicroscope (Olympus, Japan).

RNA isolation and analysis of gene expression

Total RNA was isolated from leaf tissues using WelPrepTM (JOIN BIO-INNOVATION, Daegu, Korea) and cDNA was synthesized using the ImProm IITM Reverse Transcriptase system kit (Promega, Madison, WI) as described previously with minor modifications (S2). Real-time PCR was performed using SYBR Premix Extaq (Takara, Shuzo, Kyoto, Japan) and an ABI 7300 Real-Time PCR System (Applied Biosystems, Foster City, CA). Fold changes in gene expression were calculated using the comparative C_T method, with normalized against *UBQ10* expression. Relative values of expression were determined against the maximum value of wild-type (WT). Experiments were repeated at least three times. The detailed description of the results of quantitative real-time PCRs performed in this study is summarized in table S2.

RNA gel blot analysis was performed with 40 µg, 10 µg, and 10 µg of total RNA for *ORE1*, *CAB2*, and *SAG12*, respectively. The membranes were then washed twice for 15 min with 0.2 X SSC and 0.1% SDS, after which they were placed on X-ray film. For a quantitative assay, the membranes were then exposed and analyzed with a Fuji FLA-2000 Image Analyzer (Fuji Photo Film Co. Ltd., Tokyo, Japan) and the images were processed using Science Lab 98 software (Fuji Photo Film Co. Ltd.).

Low-molecular weight RNA was isolated using the *mir*VanaTM miRNA isolation kit (Ambion, Austin, TX). Low-molecular weight RNA (20 µg) was separated by 15% denaturing polyacrylamide gel electrophoresis and was stained with EtBr. The gels were electroblotted onto Hybond-N⁺ membranes (Amersham Biosciences, Buckinghamshire, UK). A DNA oligonucleotide complementary to *miR164* was end-labeled with the *mir*VanaTM mirRNA Probe Construction Kit (Ambion) and used for hybridization. The membrane was washed with 2 X SSC, and then with 0.2X SSC and

0.1% SDS, and finally with 0.1 X SSC and 0.1% SDS. In Fig. 2A and 4B, the diluted RNA samples (200-fold dilution) were loaded and were stained with SYBR Gold for a more quantitative comparison.

Map-based cloning of the *ORE1* gene

The *ore1-1* allele was previously isolated from an EMS-mutagenized pool, and the *ore1-2* allele was isolated from a population of fast neutron-mutagenized Col seeds. Two *ore1* alleles, *ore1-1* and *ore1-2*, were inherited as monogenic recessive traits in terms of conferring the delayed leaf senescence phenotype (table S1; 8). Table S1 shows that the *ore1-1* and *ore1-2* alleles belong to a complementation group. The *ore1-2* plants were crossed with Ler plants to create mapping populations, and 1,391 plants with the mutant phenotype were selected from the F₂ progeny. Genomic DNA from each of these plants was utilized for mapping the *ORE1* locus relative to the loci of known Cleaved Amplified Polymorphic Sequence (CAPS) markers. New CAPS markers for fine mapping of the *ORE1* locus were generated in the sequence of BAC clone MIJ24: MUL8_70 (amplified with primers 5'-CAC GTT TGA TGT GTT TCT TC-3' and 5'-AAC GAC AGC TTT TTA CAG CA-3', yielding a 1.0-kb product with and without *Af*II sites in Col and Ler, respectively) and MKM21 (amplified with primers 5'-TTC AGG AGT GAC GAT ACA AG-3' and 5'-TCC ATT CTC CA A ACA TAT CA-3', yielding a 1.1 kb product with and without *Bam*HI sites in Col and Ler, respectively). The open reading frames in the vicinity of the mapped *ORE1* locus were sequenced to identify the mutated sequence.

Localization of ORE1 Protein

For transient expression in *Arabidopsis*, 5×10^4 mesophyll cell protoplasts were transfected with 40 μg of CsVMVpro:ORE1-eGFP and the control construct CsVMVpro:H2B-RFP, as described previously (S2). Protoplasts were examined using epifluorescence microscopy (AxioVert 200; Carl Zeiss). Approximately 50% of the protoplasts observed expressed *ORE1-eGFP*, and *ORE1-eGFP* was localized in the nucleus in most of the protoplasts expressing *ORE1-eGFP*.

Mathematical Modeling

A mathematical model was developed, as described in (15), as follows:

$$\begin{aligned} dmiR164/dt &= B_{miR164} - \beta_{miR164} f(ORE3^*, K_{ORE3,miR164}) - \alpha_{miR164} miR164 \\ dORE1/dt &= B_{ORE1} - \beta_{ORE1} G_1(ORE3^*, K_{ORE3,ORE1}, miR164^*, K_{miR164,ORE1}) - \alpha_{ORE1} ORE1 \\ dSAG12/dt &= B_{SAG12} - \beta_{SAG12} G_2(ORE3^*, K_{ORE3,SAG12}, ORE1^*, K_{ORE1,SAG12}) - \alpha_{SAG12} SAG12 \\ f(u, K_u) &= (u/K_u)^H / (1 + (u/K_u)^H) \text{ for an activator} \\ f(u, K_u) &= 1 / (1 + (u/K_u)^H) \text{ for a repressor} \\ G(u, K_u, v, K_v) &= f(u, K_u) f(v, K_v) \text{ for an AND gate} \end{aligned}$$

where B_{miR164} , B_{ORE1} , B_{SAG12} represent basal synthesis rates for *miR164*, *ORE1*, and *SAG12*, respectively. Similarly, α_i and β_i are degradation and production rates, respectively, of species i . The K_{ij} parameters are the activation or repression coefficient of species j by species i . The model was fit using the following parameters to the experimental data shown in fig. S8:

$$S_{ORE3} = 1 \text{ when } t \geq 8s$$

$$S_{miR164} = S_{ORE1} = 1$$

$$B_{miR164} = B_{ORE1} = B_{SAG12} = 0$$

$$\beta_{miR164} = \beta_{ORE1} = \beta_{SAG12} = 0.2$$

$$\alpha_{miR164} = \alpha_{ORE1} = \alpha_{SAG12} = 0.2$$

$$K_{ORE3,miR164} = 0.1, K_{ORE3,ORE1} = 0.5, K_{miR164,ORE1} = 0.05, K_{ORE3,SAG12} = 0.5, K_{ORE1,SAG12} = 0.5$$

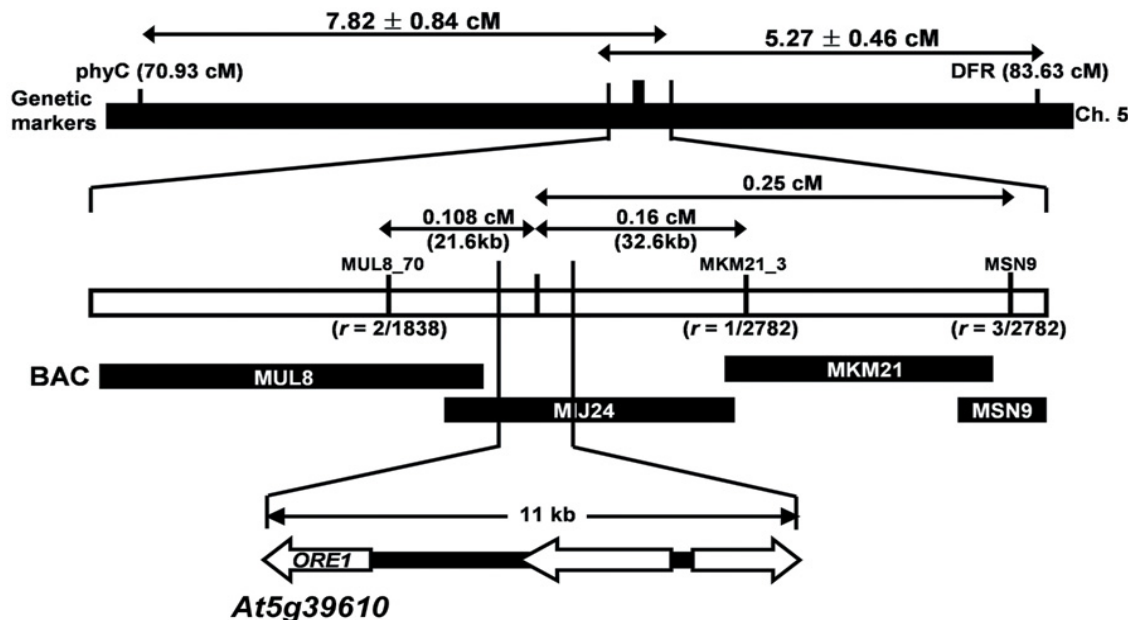


Figure S1. Map-based cloning of *ORE1* using an *ore1-2* X *Ler* F₂ population. The *ORE1* locus was positioned between *phyC* and DFR CAPS marker in Ch. 5. Fine mapping revealed that *ORE1* was located in an 11 kb region in the MIJ24 BAC. *ORE1/AtNAC2* was suggested to play a role in salt-responsive development of lateral roots (7). However, in agreement with the previous report, we also could not detect a difference in salt responses between wild-type and *ore1* mutant seedlings. While the lack of salt-responsive phenotype in the *ore1* mutant seedlings could be due to genetic redundancy, a role for *ORE1/AtNAC2* in regulation of age-induced senescence and cell death in the leaves was clearly apparent. r , the number of recombination events between the CAPS markers and the *ORE1* locus; Ch. 5, chromosome 5; BAC, bacterial artificial chromosome; cM, centimorgan.

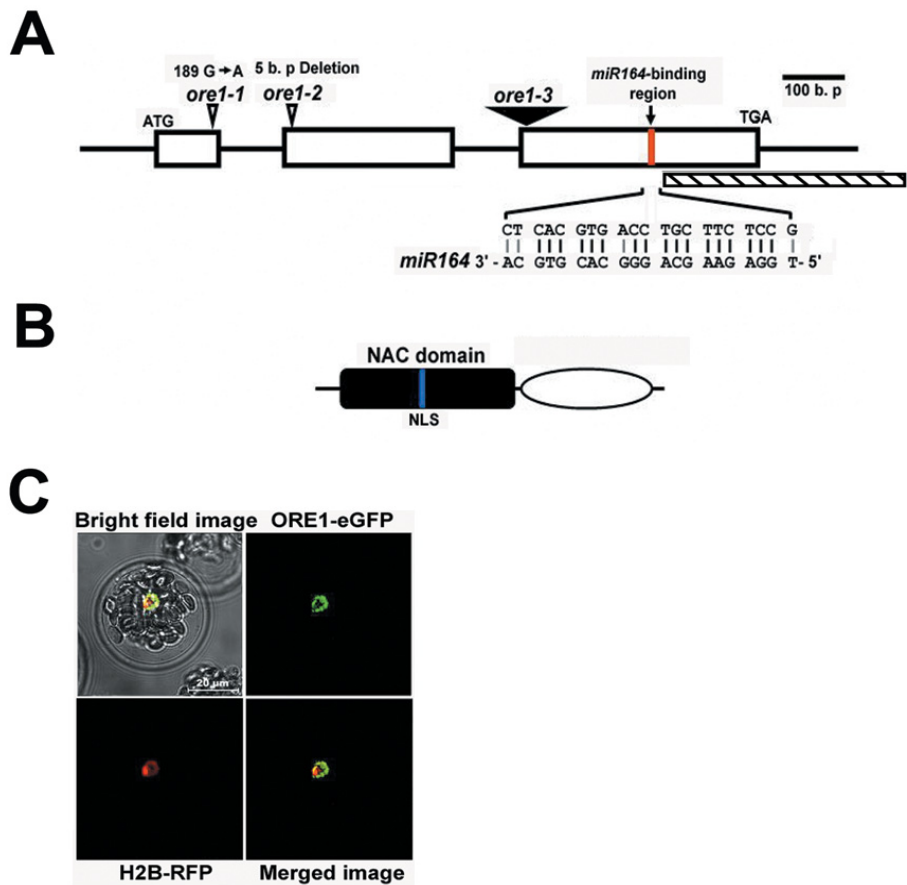


Figure S2. ORE1 is a NAC transcription factor. (A) Schematic representation of the *ORE1* gene. The 5 bp deletion in *ore1-2* occurs in the second exon and a single G to A transition in *ore1-1* occurs in the first exon. These mutations result in a premature STOP codon in the ORE1 protein sequence. A T-DNA insertion allele was also found and designated as *ore1-3*. Exons are shown as boxes. The mutated positions in the *ore1-1* and *ore1-2* alleles are indicated by arrowheads. The location of the T-DNA insertion in the *ore1-3* allele is indicated by an inverted triangle. The *miR164*-recognized region is denoted by red lines. The hatched bar represents the probe specific to the 3' region of *ORE1* used in Fig. 2A and B. (B) Structure of the *ORE1* protein. The conserved NAC domain and divergent C-terminal region are shown as a

black box and an oval, respectively. The nuclear localization sequence (NLS) is denoted by blue lines. (C) Localization of ORE1-eGFP in *Arabidopsis* protoplasts. Images show bright field, GFP, and RFP fluorescence, as well as a merged image of protoplasts transfected with CsVMVpro:ORE1-eGFP and CsVMVpro:H2B-RFP. H2B, histone 2B. Bar, 20 μ m.

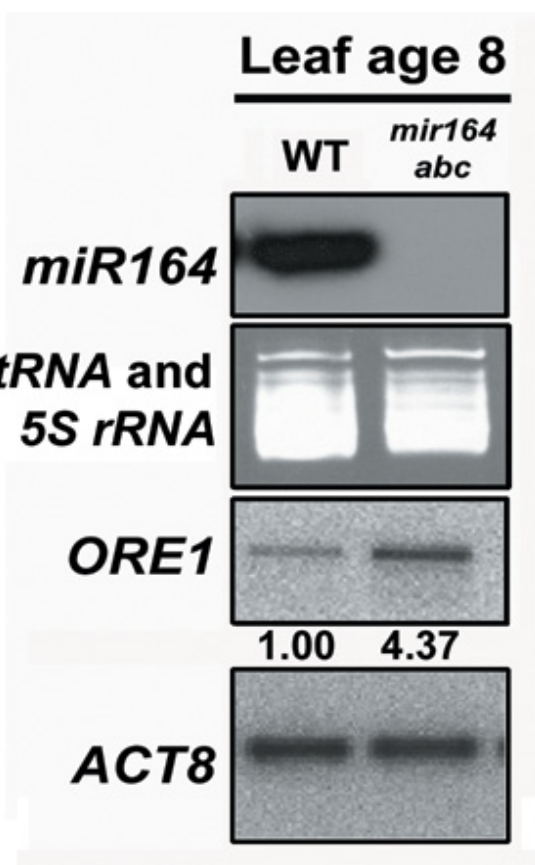


Figure S3. Expression of *miR164* and *ORE1* in 8-day-old leaves of wild-type (WT) and *mir164abc* mutant. *ORE1* transcript levels were detected by semi-quantitative RT-PCR, and were then normalized against *ACT8* (*Actin 8*) expression. Numbers indicate relative levels of *ORE1* mRNA in the *mir164abc* mutant, relative to WT. *ACT8*, loading control. PCR conditions for *ORE1* and *ACT8* were 30 cycles and 28 cycles, respectively, of 94°C for 30s, 53°C for 30s, and 72°C for 30s.

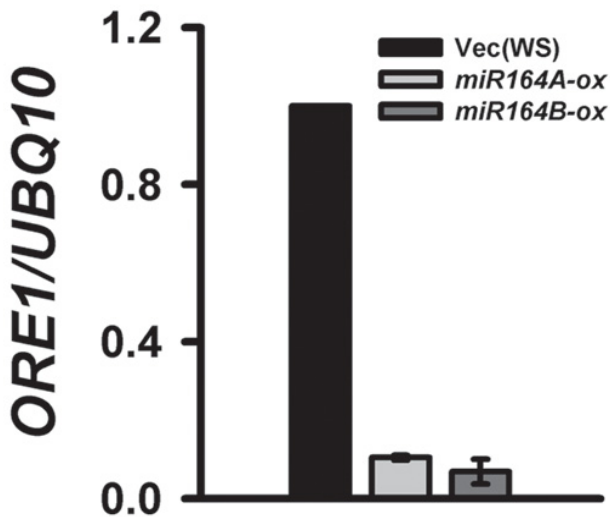


Figure S4. Expression of *ORE1* in *miR164*-overexpression lines. Level of *ORE1* mRNA in vector control (Vec), *miR164A-*, and *miR164B*-overexpressing lines in 20-day-old leaves. Transcript levels of *ORE1* were normalized against *UBQ10* expression. Values are means \pm SE ($n = 3$).

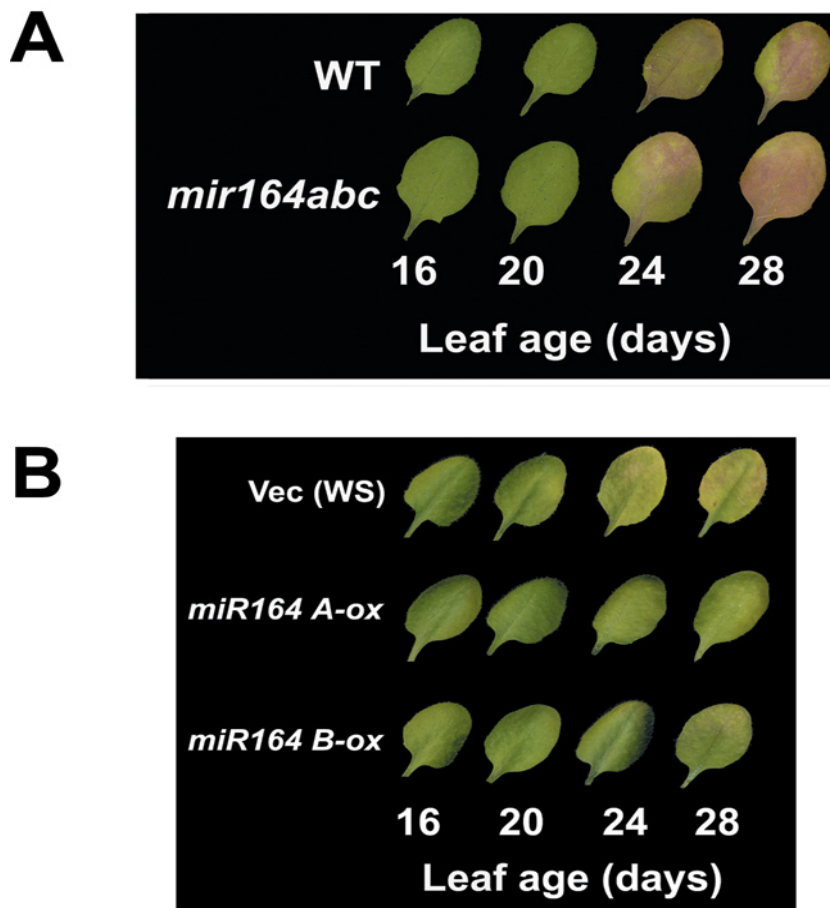


Figure S5. Age-dependent leaf senescence phenotype regulated by *miR164* expression. (A and B) Representative leaves of the *mir164abc* mutant (A) and the *miR164A*- and *miR164B*-overexpressing lines (B) with leaf aging.

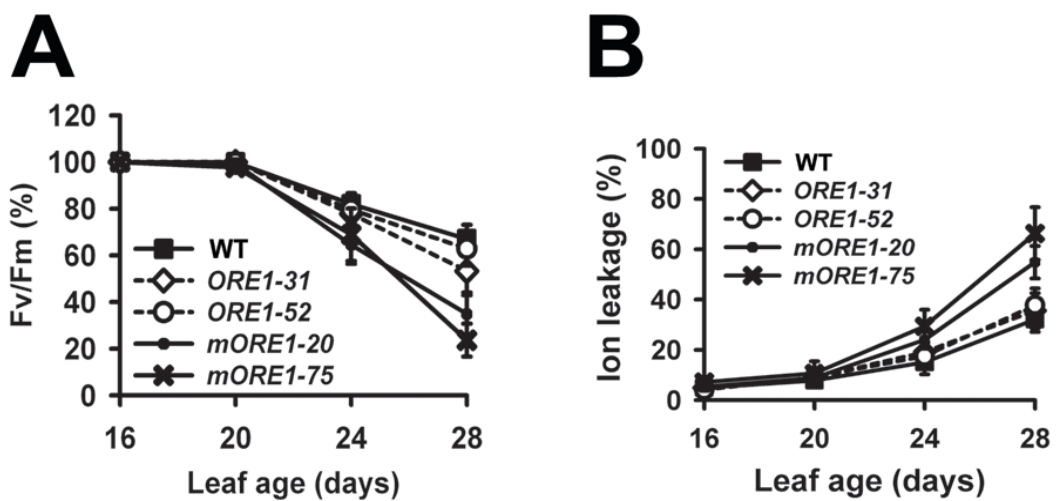


Figure S6. The mutant version of *ORE1* leads to accelerated leaf aging. (A and B) Photochemical efficiency (F_v/F_m) (A) and membrane ion leakage (B) in WT and *ORE1*- and mutant *ORE1*-overexpressing lines. Data represent the means \pm 95% confidence intervals (\pm 95 CI; $n = 18\text{--}32$).

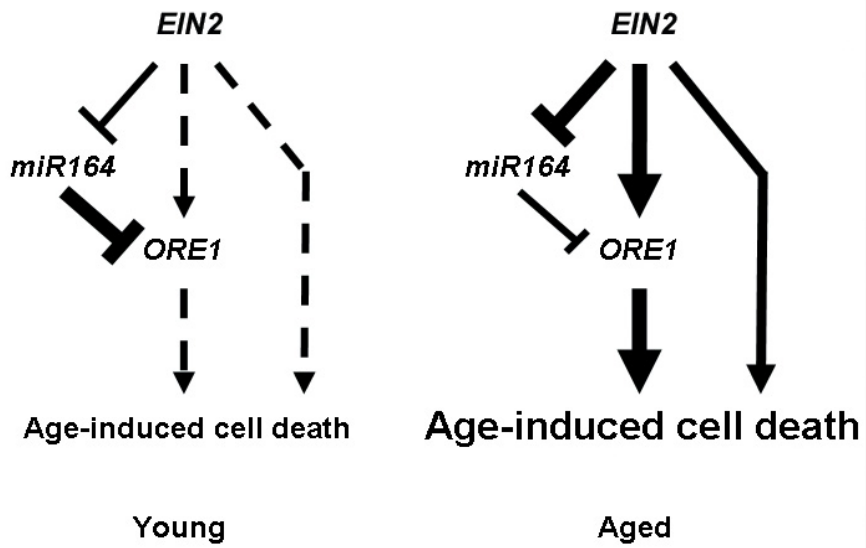


Figure S7. A trifurcate feed-forward pathway model. The model on the right depicts the regulation of age-induced cell death by *EIN2*, *miR164*, and *ORE1* in aged leaves. The regulatory model for young leaves is shown on the left.

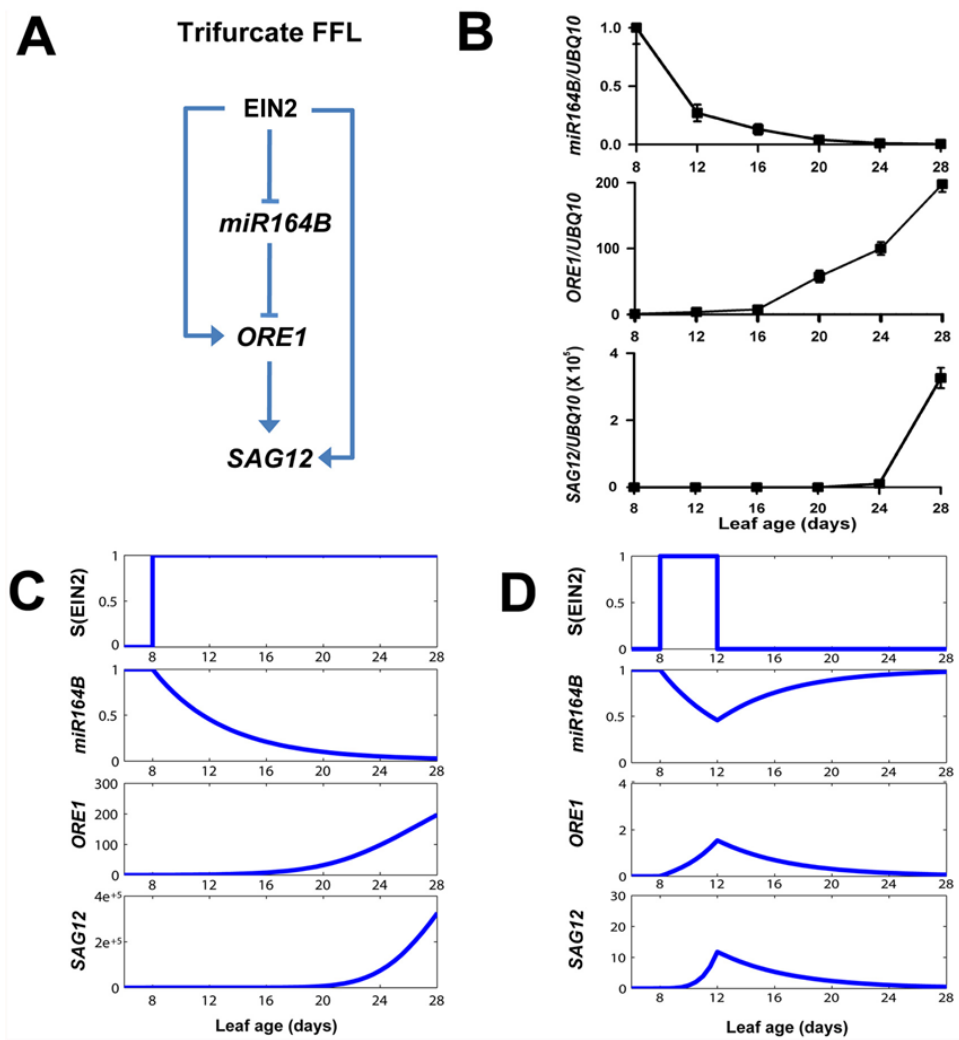


Figure S8. The dynamics of the trifurcate feed-forward pathway. (A) The trifurcate model structure developed using a mathematical model, as described in Mangan and Alon (16). (B) Sign-sensitive delays in the transcriptional induction of *ORE1* and *SAG12*, which suggest AND gate behaviors at the *ORE1* and *SAG12* junctions. Relative transcript levels of *miR164*, *ORE1*, and *SAG12* against *UBQ10* with leaf age are shown. (C) Simulation result showing the delayed responses after a systematic, persistent action of *EIN2*, using a mathematical model fitted to the experimental data of fig. S8B. *ORE1* and *SAG12* were not induced until *miR164* levels exceeded an

activation threshold, which resulted in the delayed responses. S(EIN2), activation state of EIN2. (D) Simulation result showing that *ORE1* and *SAG12* were not induced by the short-term activation of EIN2, which mimics non-systematic variations of EIN2 action, since *miR164* and *ORE1* levels did not exceed their activation thresholds.

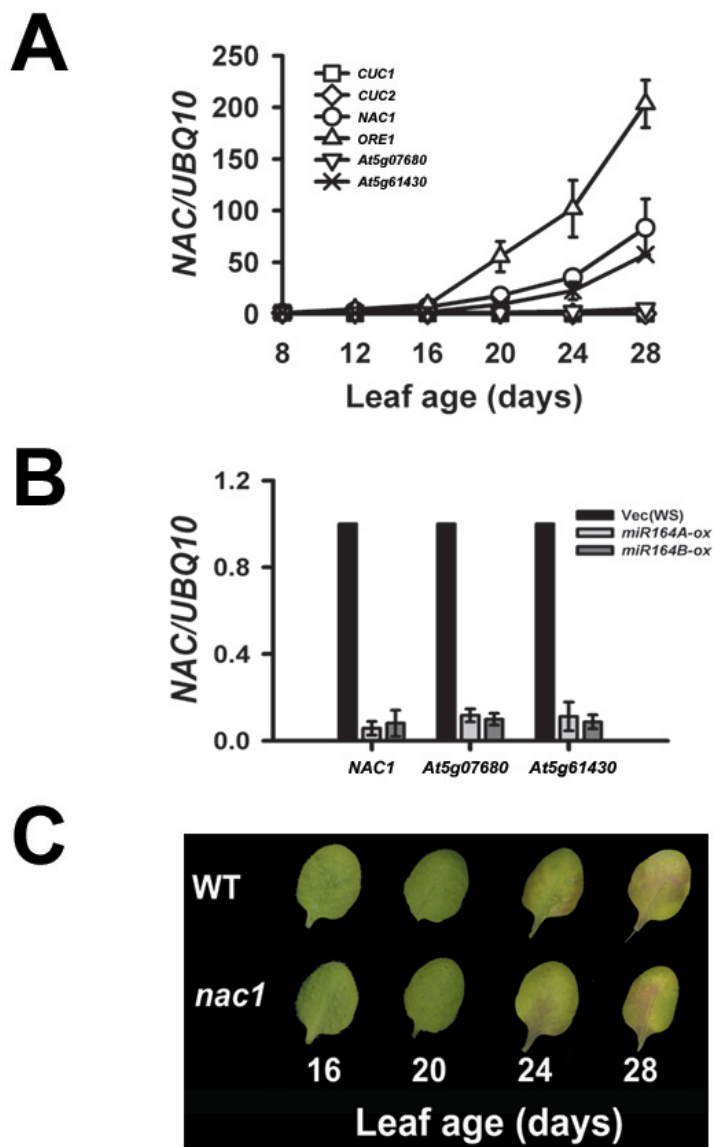


Figure S9. Age-dependent regulation of *NAC* family genes containing a *miR164*-binding sequence. (A) Expression of *NAC* family genes containing a *miR164*-binding sequence with leaf age. (B) Expression levels of *NAC1*, *At5g07680*, and *At5g61430* in vector control (Vec), *miR164A*-, and *miR164B*-overexpressing lines in 20-day-old leaves. *CUC1* and *CUC2* were not detected in any plants tested at this stage. Transcript levels of each *NAC* family gene were normalized against *UBQ10* expression. Values are means \pm SE ($n = 3$). (C) A visible leaf senescence phenotype of the T-DNA insertional mutant of *NAC1* with leaf aging.

Table S1. Complementation analyses of the *ore1* mutants. The phenotype of the progenies was scored for the senescence parameter (photochemical efficiency of Photosystem II) during age-dependent senescence. The phenotypes cosegregated in all the progeny examined. ^a+, wild-type; –, delayed senescence.

Cross	Progeny	Total	Phenotype ^a		χ^2
			+	-	
<i>ore1-2 X Col</i>	<i>F</i> ₁	48	48	0	
	<i>F</i> ₂	165	121	44	0.099 (P>0.5)
<i>ore1-2 X ore1-1</i>	<i>F</i> ₁	42	0	42	
<i>ore1-1 X ore1-2</i>	<i>F</i> ₁	28	0	28	

Table S2. Detailed description of quantitative real time PCR performed in this study. (A to G) The average and standard error of the mean in Fig. 2D (A), Fig. 2E (B), Fig. 2F (C), Fig. 3C (D), Fig. 3F (E), Fig. 4C (F), and Fig. 4E (G).

	Average		Standard error of the mean	
Vec	1.00		0	
<i>miR164B-ox</i>	0.19		0.03	
<i>ORE1-31 X Vec</i>	1.53		0.14	
<i>ORE1-31 X miR164B-ox</i>	0.26		0.12	
<i>ORE1-52 X Vec</i>	1.23		0.3	
<i>ORE1-52 X miR164B-ox</i>	0.15		0.09	
<i>mORE1-20 X Vec</i>	2.99		0.36	
<i>mORE1-20 X miR164B-ox</i>	2.50		0.21	
<i>mORE1-75 X Vec</i>	4.17		0.21	
<i>mORE1-75 X miR164B-ox</i>	3.27		0.09	

Leaf age (days)	Average		Standard error of the mean	
	WT	<i>mir164abc</i>	WT	<i>mir164abc</i>
8	1.00	3.53	0.03	0.84
12	3.01	9.46	0.72	1.48
16	12.46	21.46	4.23	2.81
20	55.42	83.80	7.56	4.95
24	109.38	125.36	8.70	8.32
28	200.96	198.79	6.62	6.40

Leaf age (days)	Average		Standard error of the mean	
	WT	<i>mir164abc</i>	WT	<i>mir164abc</i>
16	1.00	1.49	0.14	1.25
20	3.45	117.86	0.91	51.36
24	289.36	100539.68	898.88	23961.39
28	411178.48	598100.21	42525.37	51423.76

Leaf age (days)	Average			Standard error of the mean		WT
	WT	<i>mir164abc</i>	WT	<i>mir164abc</i>	WT	<i>mir164abc</i>
16	1.00	1.44	0.18	0.17	1.00	0.12
20	7.97	3.18	0.18	0.14	8.00	0.18
24	12.09	4.68	0.85	0.33	12.00	0.48
28	55.71	9.32	3.77	1.07	56.00	1.20
	107.43	26.45	11.49	0.37	110.00	1.00
	214.12	26.98	10.29	3.96	220.00	3.00

Leaf age (days)	Average					Standard error of the mean					WT	<i>ore1-1</i>	<i>ein2-34</i>
	WT	<i>ore1-1</i>	<i>ein2-34</i>	<i>ore1-1</i>	<i>ein2-34</i>	WT	<i>ore1-1</i>	<i>ein2-34</i>	<i>ore1-1</i>	<i>ein2-34</i>			
16	1.00	2.60	1.12	3.36		0.23	0.30	0.33	1.02				
20	115.97	20.36	5.69	8.69		33.42	7.79	3.14	3.08				
24	10889.44	40.79	46.19	18.01		3527.86	5.02	33.92	10.92				
28	325980.33	5295.00	104.34	52.67		30494.79	3918.53	89.59	26.41				
32		13184.74	3350.59	100.66			4938.51	3181.13	68.24				
36		205794.68	129892.79	2461.09			36641.41	30873.77	1909.40				
40				70869.32							16532.12		

References

- S1. H. R. Woo *et al.*, *Plant Cell* **13**, 1779 (2001).
- S2. J. Kim, Y. Kim, M. Yeom, J. H. Kim, H. G. Nam, *Plant Cell* **20**, 307 (2008).